ORGANIC CHEMISTRY FRONTIERS

CHINESE CHEMICAL SOCIETY

ROYAL SOCIETY OF CHEMISTRY

RESEARCH ARTICLE

View Article Online
View Journal | View Issue

Open Access Article. Published on 06 July 2020. Downloaded on 12/4/2025 7:15:25 PM.
This article is licensed under a Creative Commons Attribution-NonCommercial 3.0 Unported Licence.

Check for updates

Cite this: *Org. Chem. Front.*, 2020, **7**, 2187

π–π stacked DNA G-wire nanostructures formed by a short G-rich oligonucleotide containing a 3′–3′ inversion of polarity site†

Maria Marzano,[a] Andrea P. Falanga,[a] Principia Dardano,[b] Stefano D'Errico,[c] Ilaria Rea,[b] Monica Terracciano,[a] Luca De Stefano,[b] Gennaro Piccialli,[a] Nicola Borbone *[a] and Giorgia Oliviero[d]

Received 9th May 2020,
Accepted 12th June 2020

DOI: 10.1039/d0qo00561d

rsc.li/frontiers-organic

The interest in DNA based nanostructures arises from their potential applications in diagnostics and drug delivery and in the development of new hybrid and conducting materials. Guanine-rich oligonucleotides can multimerize forming long and stable supramolecular structures, known as G-wires, based on the G-quadruplex (G4) motif. Herein, we report a method to easily obtain long DNA G-wires based on a new tetramolecular G4 subunit formed by the d(5′-CGG-3′-3′-GGC-5′) sequence containing a 3′–3′ inversion of polarity site. The formation of the G-wire assembly exploits the multimerization ability of G4s presenting the CGG motif at their 5′ end *via* π–π stacking interactions between flanking G4 subunits. The structures and the stability of the resulting G-wires were investigated by HPLC, size exclusion chromatography, polyacrylamide gel electrophoresis, circular dichroism, ^{1}H NMR and atomic force microscopy studies.

Introduction

The discovery of new biomaterials based on ordered supramolecular structures is a hot topic in the development of nanotechnologies.[1–7] Among the various biomaterials able to build supramolecular structures, the DNA strand is a very attractive building-block having the capability of forming supramolecular complexes whose dimensions and shapes can be predicted *ab initio* by varying the length and sequence of the DNA strand.[8–11] DNA-based supramolecular structures are built by exploiting the self-assembling driving forces of DNA strands which bind to each other following simple base-pairing patterns based on Watson–Crick, Hoogsteen and reverse Hoogsteen hydrogen-bonding rules. Depending on the combination of the hydrogen bonding patterns involved, DNA strands can form predictable and well-defined secondary structures (*e.g.* duplex, triplex, DNA origami, G4).[12–14] G4s are unusual RNA and DNA secondary structures which form when G-rich ON strands are annealed in the presence of suitable cations. The binding motif of G4s is the G-quartet (Fig. 1A), a planar arrangement formed by four guanine bases held together by eight Hoogsteen hydrogen bonds.[15–17] π–π interactions generated between the stacked G-quartets and the presence of coordinating cations, such as potassium or sodium, give stability to the whole G4 structure.[18–21]

G4s are involved in many critical biological processes, including the expression of many proto-oncogenes, the maintenance of telomere length and the recognition and binding of several proteins,[22–26] and are also emerging as self-assembling scaffolds to be used in supramolecular chemistry applications and nanotechnology.[27] Furthermore, G4s possess higher conductivity than DNA duplexes, thus suggesting their use in bioelectronics.[28–31]

Supramolecular structures based on a G4 scaffold can be obtained directly through the self-assembling of the G-rich strands (Fig. 1B) or by multimerization of G4 building blocks held together by end-to-end π–π stacking (Fig. 1C). The G-wires reported, in Fig. 1B, characterized by the cooperative binding of interlocked slipped strands, have a rod-shaped superstructure that can reach the length of thousands of nanometres along the axis perpendicular to the G-tetrad planes.[32–35] The multimerization of a G4 building block is a process that produces stacked G-wires (Fig. 1C), which are supramolecular structures having a shape similar to the G-wires.[18,36–38] Other kinds of G-wires containing both these structural motifs are also reported.[39–43] The factors that influ-

[a]Department of Pharmacy, University of Naples Federico II, Via D. Montesano 49, 80131 – Naples, Italy. E-mail: nicola.borbone@unina.it
[b]Institute of Applied Sciences and Intelligent Systems, National Council Research of Italy, Via P. Castellino 111, 80131 – Naples, Italy
[c]CESTEV, University of Naples Federico II, Via T. De Amicis 95, 80145 – Naples, Italy
[d]Department of Molecular Medicine and Medical Biotechnologies, University of Naples Federico II, Via S. Pansini 5, 80131 – Naples, Italy
†Electronic supplementary information (ESI) available. See DOI: 10.1039/d0qo00561d

Open Access Article. Published on 06 July 2020. Downloaded on 12/4/2025 7:15:25 PM.
This article is licensed under a Creative Commons Attribution-NonCommercial 3.0 Unported Licence.

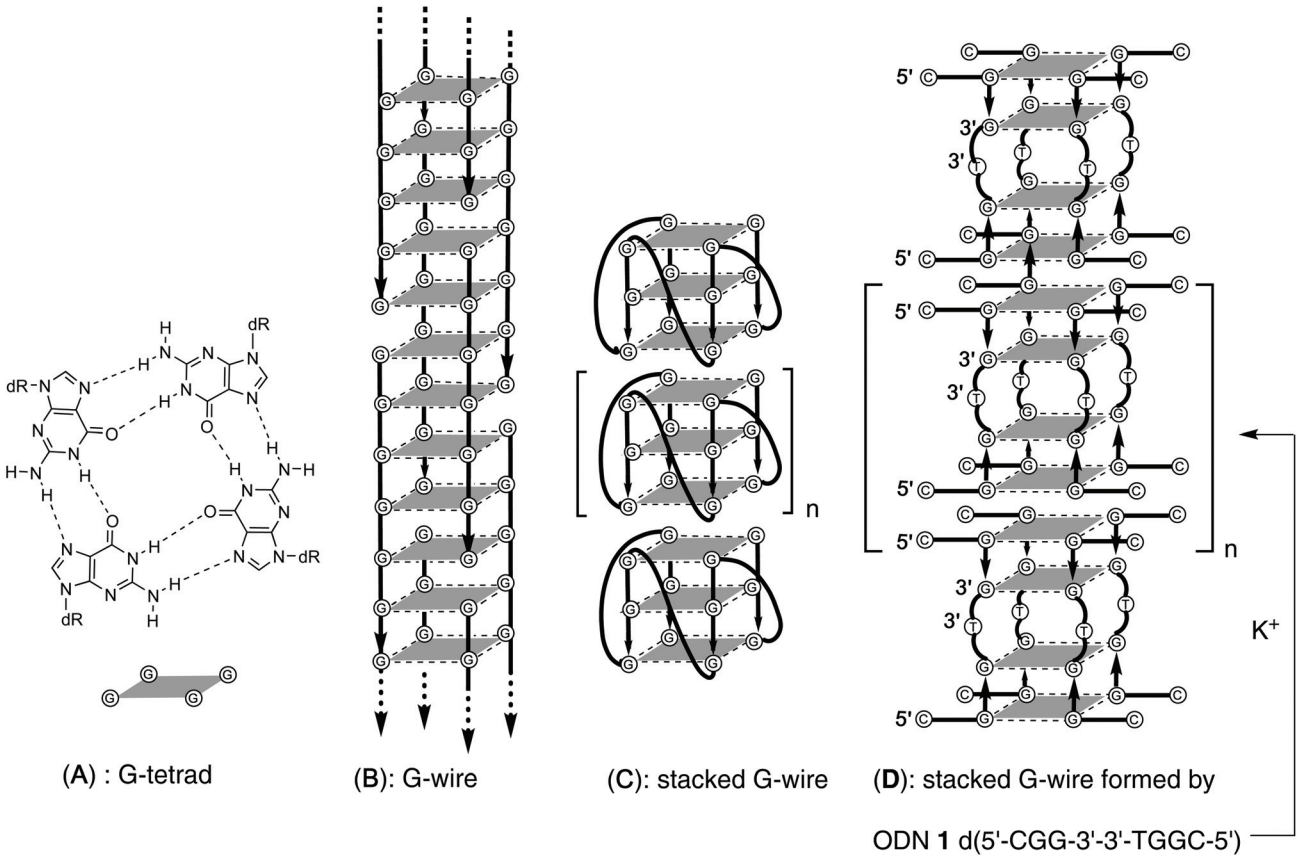

Fig. 1 Schematic representation of (A) G-tetrad, (B) interlocked G-wire, (C and D) stacked G-wires.

ence this multimerization process are: the molecularity of the G4, the base composition of the loops, the presence of overhanging nucleotides at 5′ or 3′ end of the G-rich strand, the number of G-tetrads in the G4 monomer and the kind of π–π stacking among the monomeric building blocks.[44,45]

In previous studies, we reported that the 7-mer d(CGGXGGT) (X = T, A, C, G) ONs in the presence of K^+ ions form tetramolecular $d(CGGXGGT)_4$ G4s (from here on referred as the $\mathbf{Q_1}$ monomeric building blocks) which rapidly evolve to the corresponding dimeric $\mathbf{Q_2}$ complexes *via* π–π end-stacking interaction between the unusual G(:C):G(:C):G(:C):G(:C) planar octad formed at the 5′-CGG end of each $\mathbf{Q_1}$ building block (Fig. S1, ESI†).[46,47] In a successive paper, this finding was exploited in the formation of π–π stacked G-wires (Fig. 1D) obtained through the multimerization of G4 monomeric building blocks having the 5′-CGG sticky moiety at both ends. To this aim, we synthesized the d(5′-CGGT-3′-3′-GGC-5′) (**1**, Fig. 1D) ODN sequence incorporating an inversion of polarity site at the 3′ side of the central T.[48] In this paper, we continue our study on 5′–5′ stacked G-wires, enlarging their repertoire with those formed by the shorter symmetric d(5′-CGG-3′-3′-GGC-5′) ODN sequence (**2**, Fig. 2), as demonstrated through size exclusion chromatography (HPLC-SEC), polyacrylamide gel electrophoresis (PAGE), circular dichroism (CD), ^{1}H NMR and atomic force microscopy (AFM) evidence.

The comparison of stability and length distribution between the G-wires formed by **1** and **2** revealed the crucial role played by the presence of the thymidine at the inversion of polarity site.

Results and discussion

Synthesis of d(5′-CGG-3′-3′-GGC-5′) and formation of π–π stacked G-wires

d(5′-CGG-3′-3′-GGC-5′) (**2**) was synthesized using a solid phase automated DNA synthesizer as described in the Experimental section. The 3′–3′ phosphodiester bond was achieved by performing the first three coupling cycles using 5′-phosphoramidites, and the remaining three using standard 3′-phosphoramidites. After purification by HPLC in a SAX column, the structure and purity of **2** were confirmed by ESI MS data and ^{1}H NMR spectroscopy. In particular, the enhanced resolution ESI-MS spectrum of **2** showed a single peak corresponding to the single-stranded double-charged pseudomolecular ion $[M - 2H]^{2-}$ (m/z 915.0, Fig. S2†). The ^{1}H NMR spectrum recorded at 50 °C showed the expected three aromatic and three anomeric proton signals because of the symmetric nature of the ODN sequence (Fig. S3†). The G4 building block **3** and the G-wire **4** (Fig. 2), from now on respectively referred as $\mathbf{Q_1}$ and $\mathbf{Q_n}$, were

Open Access Article. Published on 06 July 2020. Downloaded on 12/4/2025 7:15:25 PM.
This article is licensed under a Creative Commons Attribution-NonCommercial 3.0 Unported Licence.

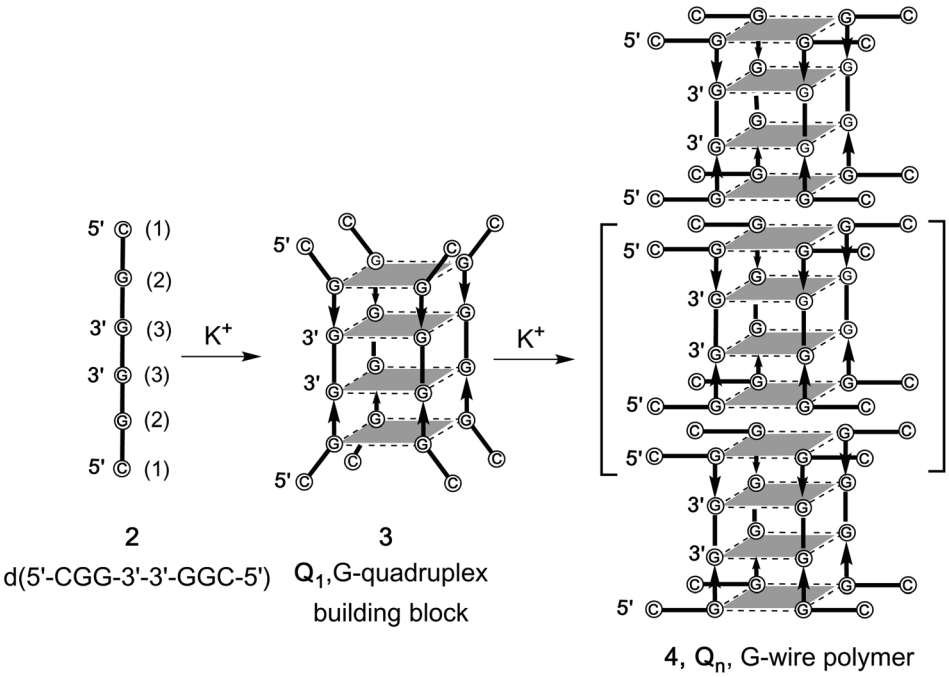

Fig. 2 Formation of the G-quadruplex building block **3** ($\mathbf{Q_1}$) and its multimerization into G-wire polymers **4** ($\mathbf{Q}_n$) starting from **2**.

obtained by dissolving **2** in 1.0 M K^+-containing buffer at the single strand (ss) concentration of 0.05, 1.0 and 3.6 mM followed by heating at 90 °C for 10 min, fast cooling at 4 °C and storage for 24 before further investigation. The formation of $\mathbf{Q_1}$ and its dimer $\mathbf{Q_2}$ was also confirmed by ESI-MS spectrometry which showed multicharged peaks corresponding to the G4 species stabilized respectively by three or six ammonium ions (Fig. S4†).

Polyacrylamide gel electrophoresis (PAGE) studies

ODN **2** after the annealing procedure was analyzed by PAGE to investigate on the G4 formation and its multimerization to form the $\mathbf{Q}_n$ multimers. We compared the electrophoretic mobility of **2** (lane 3 and 4, in Fig. 3A) with those of the G4s $d(TGGGGT)_4$ (lane 1) and $d(CGGTGGT)_8$ (lane 2), used as size markers for the G4 building block $\mathbf{Q_1}$ and its dimer $\mathbf{Q_2}$, respectively. ODN **2** annealed at 1.0 mM ODN single strand concentration in 1.0 M K^+ buffer migrated as a well-defined ladder of bands (lane 3) in which the shorter terms of the $\mathbf{Q}_n$ polymer ($\mathbf{Q_{1-4}}$) could be identified. The fastest band (lane 3) migrated with almost the same mobility as the G4 monomer marker (lane 1) and was attributed to the $\mathbf{Q_1}$ species (**3**, Fig. 2) also considering the DNA ladder reference (lane 5). As expected, $\mathbf{Q_2}$ species (48 nucleotides) migrated a little faster than the dimer marker (lane 2, 56 nucleotides). Furthermore, we observed that the efficiency and progression of the polymerization process of **2** depend on its concentration. When **2** was annealed at 0.05 mM in the same buffer, it showed a different distribution of the multimers (lane 4), in which only the first three terms ($\mathbf{Q_{1-3}}$) of the G-wires distribution could be clearly observed.

These data strongly suggest that **2** in the presence of K^+ ions self-assembles to give a distribution of G-wire species of different length (**4**, Fig. 2) by the sequential 5′-stacking of the symmetrical tetramolecular G4 building block **3**. The PAGE in Fig. 3B reports the comparison between the electrophoretic mobility of the G-wires formed by **1** and **2**. As expected, all bands formed by the longer (7-mer) ODN **1** had lower mobility than the corresponding bands formed by the shorter (6-mer) ODN **2**.

Size exclusion chromatography (SEC) studies

The G-wires distribution formed by **2** was further analyzed by size exclusion chromatography at room temperature on a Yarra 2000 HPLC-SEC column. The HPLC profile of **2** annealed at 1.0 mM ss concentration in 1.0 M K^+-containing buffer is reported in Fig. 4B. It showed a distribution of peaks in which lower molecular weight species had greater retention times.

As molecular weight markers, we used d(T6), $d(TGGGGT)_4$ and $d(CGGTGGT)_8$ respectively for the single-stranded ODN and for the monomeric ($\mathbf{Q_{1*}}$) and dimeric ($\mathbf{Q_{2*}}$) G4 assemblies (Fig. 4D). The above mentioned HPLC profiles indicated that in the reported conditions **2** forms a distribution of $\mathbf{Q}_n$ multimers composed by all members of the series with $n \leq 7$. Longer G-wires ($n > 7$) and the ss ODN were present only as traces (Fig. 4B). The HPLC-SEC analysis of the multimers formed annealing ODN **2** at lower concentration (0.05 mM ss concentration, Fig. 4A) agreed well with the PAGE data. Only three peaks ($\mathbf{Q_{1-3}}$) were observed, thus indicating that the polymerization process is slow at lower ODN concentrations. When **2** was annealed at 3.6 mM ss concentration, we saw, as expected, the shift towards higher molecular weight species of

Open Access Article. Published on 06 July 2020. Downloaded on 12/4/2025 7:15:25 PM.
This article is licensed under a Creative Commons Attribution-NonCommercial 3.0 Unported Licence.

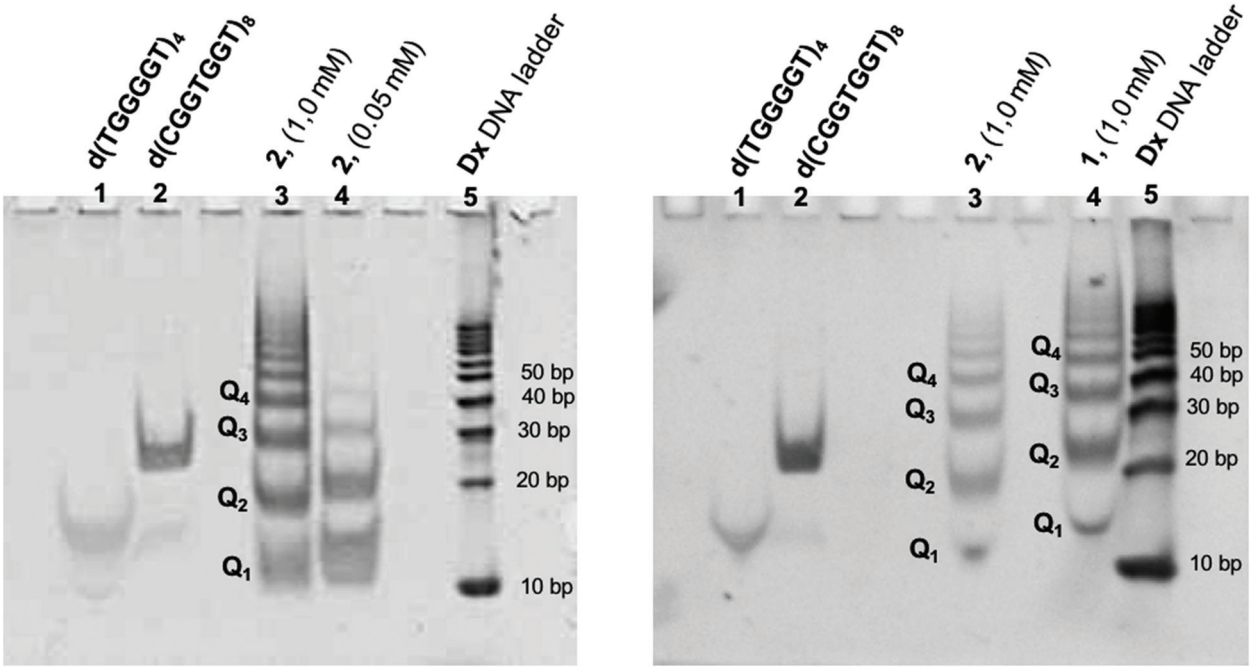

Fig. 3 (A) Electrophoretic mobility of ODNs assessed 24 h after annealing in 1.0 M K^+ buffer and storage at 4 °C. Lane 1: $d(TGGGGT)_4$; lane 2: $d(CGGTGGT)_8$; lane 3: **2** (1.0 mM ss conc.); lane 4: **2** (0.05 mM ss conc.); lane 5: duplex DNA ladder scale. (B) Comparison of the $\mathbf{Q}_n$ distribution formed by **2** (lane 3) and **1** (lane 4).

the $\mathbf{Q}_n$ distribution (Fig. 4C). Neither of the HPLC profiles showed in Fig. 4A–C changed prolonging the annealing time of the injected sample up to 48 h and 72 h, thus suggesting that in those conditions the polymerization–depolymerization process reaches an equilibrium within the first 24 h from the annealing (data not shown). We also tested the capability of ODN **2** to form $\mathbf{Q}_n$ multimers in the presence of NH_4^+ and Na^+ cations. In both cases, we detected a slower but similar polymerization process that was monitored by HPLC-SEC and PAGE experiments (data not shown). To assess the purity and stability at time and temperature of the shorter members of the $\mathbf{Q}_n$ distribution **4**, we collected the HPLC-SEC peaks of $\mathbf{Q}_{1-3}$ and stored them at r.t. in the collected eluent. Each isolated peak was reinjected in the same conditions 30 min or 24 h after the isolation to check the propensity to convert either into higher or lower M.W. assemblies (Fig. S5†). The results revealed that $\mathbf{Q}_1$ was obtained as an almost pure species that remained stable for 24 h when only a little amount of the $\mathbf{Q}_2$ species (5%) was observed. On the contrary, the reinjection of $\mathbf{Q}_2$ and $\mathbf{Q}_3$ 30 min after their isolation disclosed the formation of shortening fragments, whose amounts increased considerably after 24 h. In any case, we did not observe the re-formation of the single strand **2**. The effect of the temperature on the distribution of $\mathbf{Q}_n$ multimers formed by **2** was studied by injecting the annealed **2** before and after its heating at 45, 65 and 85 °C (Fig. S6B†), and the results were compared with the corresponding data reported for $\mathbf{Q}_n$ multimers formed by **1** (Fig. S6A†).[41] In both cases, the heating induced the melting of longer G-wires with the concomitant increase of the G4 monomer $\mathbf{Q}_1$. However, we observed a noteworthy difference in the amount of ss species formed by the two ODNs. In the HPLC-SEC profile of **1**, the most retained peak corresponding to the ss ODN was observed at all the studied temperatures and represented the most intense or the only relevant peak respectively at 65 and 85 °C (Fig. S6A†). Conversely, in the case of **2**, we did not observe a significant amount of the ss species even at 85 °C, where $\mathbf{Q}_1$ and $\mathbf{Q}_2$ were the sole observable species in the 5 : 1 ratio. The HPLC-SEC study evidenced the higher thermal stability of the G4 monomer formed by **2**, likely due to the absence of the central thymine base that, instead, weakens the G-tetrads stacking in the corresponding G4 building block formed by **1**.

Circular dichroism (CD)

CD spectroscopy furnishes useful information about the formation and topology of G4s. It is well documented that the CD profiles of parallel G4s display a maximum around 265 nm and a minimum around 240 nm; while those of antiparallel G4s show a maximum around 295 nm and a minimum around 260 nm. These profiles result mainly from the different combination of the glycosidic bond conformation of guanosines participating in the G-tetrad core. In parallel G4s all guanosines engaged in a G-tetrad adopt the *anti* conformation, whereas in antiparallel G4s they adopt alternating *syn–anti* glycosidic bond conformation along the stem.[18,49–51] In the case of $\mathbf{Q}_n$ formed by **2**, we observed a CD profile that results from the peculiar structural features of these structures, *i.e.* the presence of a 3′–3′ inversion of polarity site in the G4-forming ODN

 This journal is © the Partner Organisations 2020

Open Access Article. Published on 06 July 2020. Downloaded on 12/4/2025 7:15:25 PM.
This article is licensed under a Creative Commons Attribution-NonCommercial 3.0 Unported Licence.

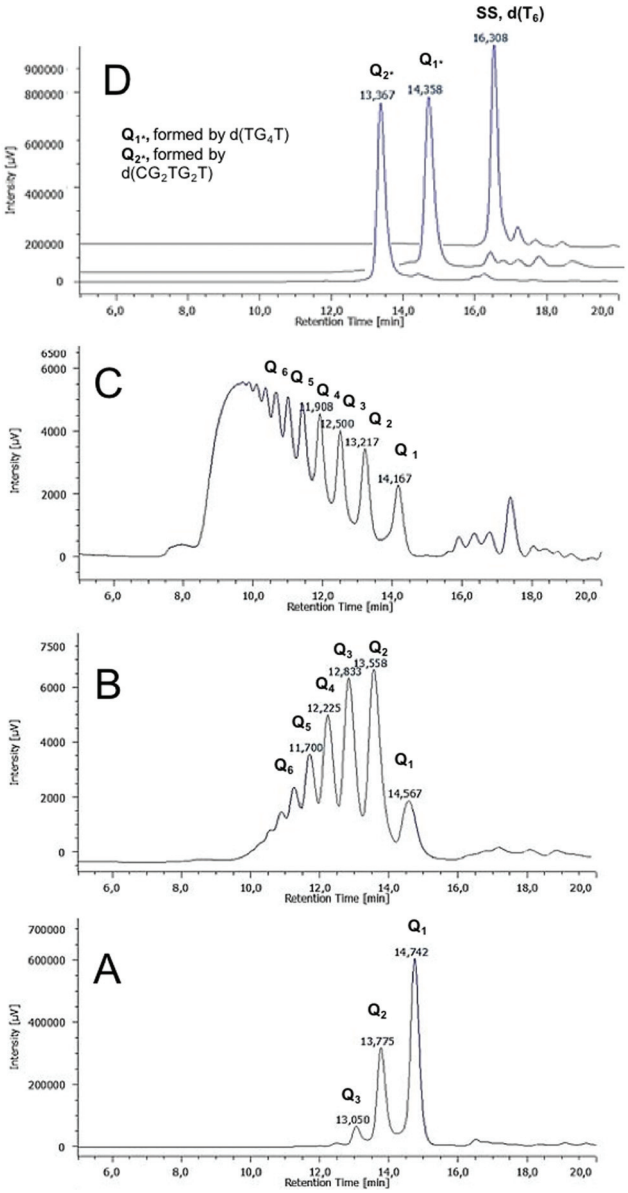

Fig. 4 HPLC-SEC profiles of $\mathbf{Q}_n$ distributions obtained by annealing **2** at (A) 0.05 mM, (B) 1.00 mM and (C) 3.60 mM. (D) HPLC-SEC profiles of the single strand (dT_6), G4 monomer ($\mathbf{Q_{1*}}$) and G4 dimer ($\mathbf{Q_{2*}}$) markers.

and the π–π stacking between the 5′-ending octads belonging to the different G4 building blocks participating in the formation of $\mathbf{Q}_n$ G-wires.

The CD profile of the $\mathbf{Q}_n$ distribution showed positive signals at 250 and 300 nm and negative signals at 230 and 280 nm (Fig. 5), in agreement with those reported for the $\mathbf{Q}_n$ multimer formed by **1**[48] and the G4 formed by d(5′-TGG3′-3′ GGT-5′),[52] both containing a 3′–3′ inversion of polarity site in the ODN sequence. We also recorded the CD spectra of the HPLC-SEC peaks corresponding to $\mathbf{Q_1}$, $\mathbf{Q_2}$ and $\mathbf{Q_3}$, as well as that of all other less-retained peaks collected together ($\mathbf{Q}_{4-n}$), to assess the influence of the degree of multimerization on the CD signature of $\mathbf{Q}_n$ assemblies (Fig. 6).

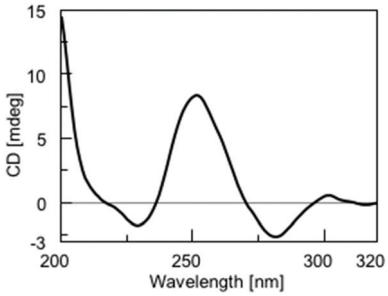

Fig. 5 CD spectrum recorded at 25 °C of the $\mathbf{Q}_n$ distribution obtained by annealing **2** in 100 mM K^+ buffer.

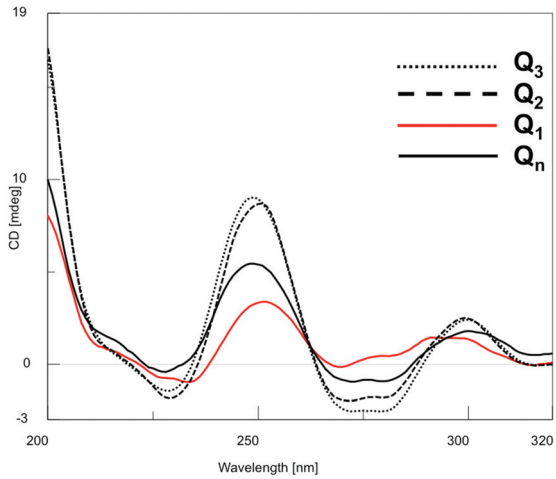

Fig. 6 CD spectra of $\mathbf{Q_1}$, $\mathbf{Q_2}$, $\mathbf{Q_3}$ and $\mathbf{Q}_{4-n}$ species isolated from the HPLC-SEC fractionation showed in Fig. 4B.

The results confirmed the G4 nature of all the eluted species, as well as the absence of significant perturbations due to polymerization/depolymerization equilibria. To estimate the thermal behavior of the $\mathbf{Q}_n$ distribution formed by **2**, we performed CD melting experiments. The melting curve recorded at 252 nm (Fig. S4†) well evidenced that the G-wires formed by **2** are stable at room temperature and start to disassemble at temperatures higher than 30 °C. The presence of three to four inflection points in the curve disclosed the progressive shortening of the G-wire assembly. Considering that the melting process was not complete even at 90 °C, we attributed the last observed inflection point (at around 75 °C) to the formation of the $\mathbf{Q_1}$ building block which, differently from the corresponding $\mathbf{Q_1}$ species formed by **1**, did not melt in the explored temperature range.

Nuclear magnetic resonance (NMR)

^{1}H NMR spectroscopy is an important technique to investigate the formation, the stability and the topology of G4s. The downfield region of water-suppressed ^{1}H NMR spectra of G4s is characterized by the presence of the diagnostic exchange-protected H1 imino protons of guanine bases engaged in

Open Access Article. Published on 06 July 2020. Downloaded on 12/4/2025 7:15:25 PM.
This article is licensed under a Creative Commons Attribution-NonCommercial 3.0 Unported Licence.

G-tetrads formation. These protons do not exchange with water solvent protons because of the hydrogen bond which they form with either the O6 or N7 atom of the G-tetrad flanking guanosine (Fig. 1A).[51,53] Each G-tetrad can originate one, two or four imino proton signals, depending on the magnetic equivalence of the four participating imino protons.[54] This magnetic behavior arises from the symmetry of the whole G4 structure and the *N*-glycosidic torsion angles. Fig. S5† shows the downfield regions of the water suppressed ^{1}H NMR spectra (recorded at 25, 45, 65 and 85 °C) of the $\mathbf{Q}_n$ distribution obtained by annealing **2** at 1.5 mM ss concentration in 1.0 M K^+-containing buffer. The presence of many imino protons signals in the 10.6–11.5 ppm region confirmed the existence of G4 species in all the explored temperature range. The great number of the observed signals was somewhat unexpected, considering the symmetric nature of the $\mathbf{Q_1}$ building block (**3** in Fig. 2) and the previously reported NMR spectrum of d(5′-TGG3′-3′GGT-5′) which showed only two imino proton signals[52] (thus confirming the magnetic equivalence of G-tetrads belonging to the two halves of the G4). However, taking into account the previously reported NMR data regarding the formation of the G4 dimer by the 5′-TGGAGGT-3′ ODN sequence, which evidenced modifications in the resonance frequency of all G4 imino protons before and after G4 dimerization,[47] we believe that the exchange-protected signals observed at 25, 45 and 65 °C in Fig. S5† can be attributed to the G-tetrads imino protons of stacked polymeric $\mathbf{Q}_n$ species. This hypothesis was further corroborated by the general reduction in the number and intensity of imino signals heating the sample from 25 to 85 °C as a consequence of the thermally induced transition from the $\mathbf{Q}_n$ polymer to the monomeric $\mathbf{Q_1}$ building block, in agreement with HPLC-SEC and CD data. Indeed, in the NMR spectrum recorded at 85 °C, we observed only the two expected imino signals belonging to the two couples of symmetric G-tetrads in **3**, thus confirming the higher thermal stability of the $\mathbf{Q_1}$ formed by ODN **2** with respect to the $\mathbf{Q_1}$ obtained from ODN **1**, which resulted completely melted at that temperature.[48]

Atomic force microscopy (AFM)

AFM is a powerful technique successfully used to explore the various topologies of G-wire.[35,55,56] By using this technique, we investigated the morphology of the $\mathbf{Q}_n$ G-wire species obtained from **2** annealed in 1.0 M K^+ buffer. We used muscovite mica as the AFM support both for the super-hydrophilic property of its surface, that guarantees a lower interaction between suspended molecules in aqueous solution during the evaporation of the solvent, and for its flatness (less than 0.5 nm of root mean-square roughness for a 1000 × 1000 nm^2 surface area). AFM images in Fig. 7 shows the typical arrangements of $\mathbf{Q}_n$ multimers formed by ODN **2**; in particular, Non-Contact Mode (NCM) amplitude (left) and phase (right) reveal a kind of elementary units that arranges in formations of linear shape. The analysis of a wider AFM field (Fig. S6†) disclosed the presence of more than 300 rod-shaped structures having several lengths (10–400 nm) but sharing the same height (1.8 ± 0.2 nm) and a mean width of 21 ± 7 nm (the statistical analysis is reported in Fig. S6†). The AFM length measurements are compatible with the hypothesized G-wire polymers formed by $\mathbf{Q}_n$ multimers of different length. Moreover, the homogeneity of height values of aggregates agrees with the width value of the $\mathbf{Q_1}$ building block, suggesting the formation of self-assembled G-wires monolayers only in the x-y plane. Though slightly smaller than expected, the height of the $\mathbf{Q}_n$ aggregates formed by **2** agrees with the AFM data of the G-wires obtained from **1** (height 2.0 nm),[48] and lies in the range of heights reported in the literature for the G-wires (1.5–3.5 nm)[35,43,56,57] which is usually smaller than the solution diameter of G4s (about 2.8 nm). Differently from height measurements, the curvature radius of the AFM tip affects the length and width measurements. We believe that the curvature radius of the AFM tip and the evaporation of the buffer solution, which could promote the lateral aggregation of $\mathbf{Q}_n$ multimers, are

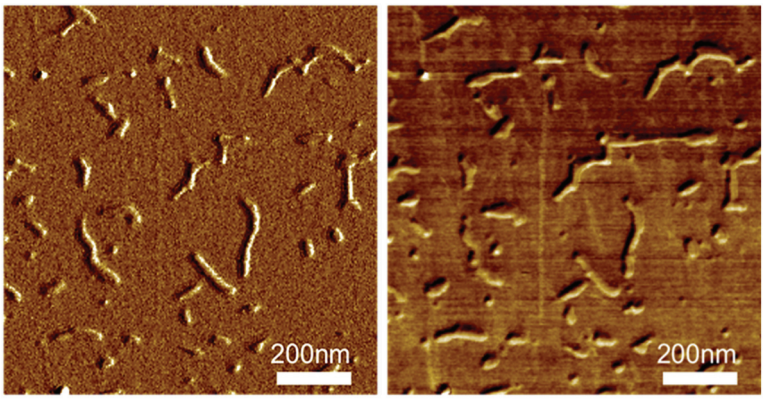

	Length (nm)	Wideness (nm)	Highness (nm)
Mean	83.85	21.21	1.76
Std.	60.96	6.53	0.18

Fig. 7 AFM imaging of $\mathbf{Q}_n$ multimers formed by ODN **2**: non-contact mode (NCM) amplitude (left) and phase (right) of the sample.

 This journal is © the Partner Organisations 2020

Open Access Article. Published on 06 July 2020. Downloaded on 12/4/2025 7:15:25 PM.
This article is licensed under a Creative Commons Attribution-NonCommercial 3.0 Unported Licence.

both responsible for the larger width of the G-wire filaments observed in the AFM field (21 ± 7 other than the expected 2.0 nm).

Conclusions

The here reported results demonstrate that rod-shaped G4 assemblies can also be easily obtained by annealing the symmetric 6-mer ODN sequence d(5′-CGG-3′-3′-GGC-5′) (**2**) in K^+- and NH_4^+-containing buffers. We selected the ODN **2** because it represented the shortest possible ODN sequence possessing the 5′-CGG moiety at both ends of the ODN strand which in our previous studies allowed the obtainment of G4 multimers *via* π–π end-stacking interactions. The thermal stability of the G4 building block **3** and the length distribution of the resulting G4 multimers were compared with those of the corresponding G4 structures obtained from the closest related longer analogue d(5′-CGGT-3′-3′-GGC-5′) (**1**) ODN. The results of this comparative study indicated that the thermal stability and length distribution of the obtained G-wires depend on the thermal stability of the G4 building block, which in turn depends on the sequence of the annealed G-rich ODN. The data indicated that the more stable is the G4 building block, the less stable is the resulting G-wire polymer. This finding suggests that it is possible to build stacked G-wires with customizable stability by varying the length and sequence of the parent ODN. In summary, our results contribute to the understanding of the processes that govern the multimerization of G-quadruplexes and extend the DNA toolbox for the construction of self-assembled supramolecular entities.

Conflicts of interest

There are no conflicts to declare.

Acknowledgements

This project was supported in part by MIUR PRIN 2017 project 2017YJMPZN.

Notes and references

1 L. Yang, X. Tan, Z. Wang and X. Zhang, Supramolecular Polymers: Historical Development, Preparation, Characterization, and Functions, *Chem. Rev.*, 2015, **115**, 7196–7239.
2 L. Wang, C. Gong, X. Yuan and G. Wei, Controlling the Self-Assembly of Biomolecules into Functional Nanomaterials through Internal Interactions and External Stimulations: A Review, *Nanomaterials*, 2019, **9**, 285.
3 G. A. Ozin, K. Hou, B. V. Lotsch, L. Cademartiri, D. P. Puzzo, F. Scotognella, A. Ghadimi and J. Thomson, Nanofabrication by Self-Assembly, *Mater. Today*, 2009, **12**, 12–23.
4 E. Busseron, Y. Ruff, E. Moulin and N. Giuseppone, Supramolecular Self-Assemblies as Functional Nanomaterials, *Nanoscale*, 2013, **5**, 7098–7140.
5 M. Martín-Arroyo, A. Prado, R. Chamorro, N. Bilbao and D. González-Rodríguez, Elucidating Noncovalent Reaction Mechanisms: G-Quartet as an Intermediate in G-Quadruplex Assembly, *Angew. Chem., Int. Ed.*, 2020, **59**, 9041–9046.
6 V. Vázquez-González, M. J. Mayoral, R. Chamorro, M. M. R. M. Hendrix, I. K. Voets and D. González-Rodríguez, Noncovalent Synthesis of Self-Assembled Nanotubes through Decoupled Hierarchical Cooperative Processes, *J. Am. Chem. Soc.*, 2019, **141**, 16432–16438.
7 P. S. Kwon, S. Ren, S. J. Kwon, M. E. Kizer, L. Kuo, M. Xie, D. Zhu, F. Zhou, F. Zhang, D. Kim, *et al.*, Designer DNA architecture offers precise and multivalent spatial pattern-recognition for viral sensing and inhibition, *Nat. Chem.*, 2020, **12**, 26–35.
8 F. Hong, F. Zhang, Y. Liu and H. Yan, DNA Origami: Scaffolds for Creating Higher Order Structures, *Chem. Rev.*, 2017, **117**, 12584–12640.
9 Y. Cao, Y. Kuang, L. Yang, P. Ding and R. Pei, Construction of One- and Two-Dimensional Nanostructures by the Sequential Assembly of Quadruplex DNA Scaffolds, *Biomacromolecules*, 2019, **20**, 2207–2217.
10 N. C. Seeman and H. F. Sleiman, DNA nanotechnology, *Nat. Rev. Mater.*, 2018, **3**, 17068.
11 P. W. K. Rothemund, Folding DNA to create nanoscale shapes and patterns, *Nature*, 2006, **440**, 297–302.
12 S. Kogikoski, W. J. Paschoalino and L. T. Kubota, Supramolecular DNA Origami Nanostructures for Use in Bioanalytical Applications, *TrAC, Trends Anal. Chem.*, 2018, **108**, 88–97.
13 A. E. Marras, L. Zhou, H.-J. Su and C. E. Castro, Programmable Motion of DNA Origami Mechanisms, *Proc. Natl. Acad. Sci. U. S. A.*, 2015, **112**, 713–718.
14 V. Linko and H. Dietz, The Enabled State of DNA Nanotechnology, *Curr. Opin. Biotechnol.*, 2013, **24**, 555–561.
15 S. Burge, G. N. Parkinson, P. Hazel, A. K. Todd and S. Neidle, Quadruplex DNA: Sequence, Topology and Structure, *Nucleic Acids Res.*, 2006, **34**, 5402–5415.
16 H. L. Lightfoot, T. Hagen, N. J. Tatum and J. Hall, The Diverse Structural Landscape of Quadruplexes, *FEBS Lett.*, 2019, **593**, 2083–2102.
17 S. Kolesnikova and E. A. Curtis, Structure and Function of Multimeric G-Quadruplexes, *Molecules*, 2019, **24**, 3074.
18 N. Smargiasso, W. Hsia, P. Colson, E. S. Baker, M. T. Bowers and E. De Pauw, G-Quadruplex DNA Assemblies: Loop Length, Cation Identity, and Multimer Formation, *J. Am. Chem. Soc.*, 2008, **135**, 10208–10216.
19 A. Risitano and K. R. Fox, Influence of Loop Size on the Stability of Intramolecular DNA Quadruplexes, *Nucleic Acids Res.*, 2004, **32**, 2598–2606.
20 P. L. T. Tran, A. De Cian, J. Gros, R. Moriyama and J.-L. Mergny, Tetramolecular Quadruplex Stability and Assembly, *Top. Curr. Chem.*, 2013, **330**, 243–273.

Open Access Article. Published on 06 July 2020. Downloaded on 12/4/2025 7:15:25 PM.
This article is licensed under a Creative Commons Attribution-NonCommercial 3.0 Unported Licence.

21 D. Pavc, B. Wang, L. Spindler, I. Drevenšek-Olenik, J. Plavec and P. Šket, Ends Control Topology of DNA G-Quadruplexes and Their Cation-Dependent Assembly, *Nucleic Acids Res.*, 2020, **48**, 2749–2761.

22 D. Rhodes and H. J. Lipps, Survey and Summary G-Quadruplexes and Their Regulatory Roles in Biology, *Nucleic Acids Res.*, 2015, **43**, 8627–8637.

23 G. Biffi, D. Tannahill, J. McCafferty and S. Balasubramanian, Quantitative Visualization of DNA G-Quadruplex Structures in Human Cells, *Nat. Chem.*, 2013, **5**, 182–186.

24 C. Platella, C. Riccardi, D. Montesarchio, G. N. Roviello and D. Musumeci, G-Quadruplex-Based Aptamers against Protein Targets in Therapy and Diagnostics, *Biochim. Biophys. Acta, Gen. Subj.*, 2016, **1861**, 1429–1447.

25 C. Roxo, W. Kotkowiak and A. Pasternak, G-Quadruplex-Forming Aptamers—Characteristics, Applications, and Perspectives, *Molecules*, 2019, **24**, 3781.

26 A. P. Falanga, V. Cerullo, M. Marzano, S. Feola, G. Oliviero, G. Piccialli and N. Borbone, Peptide Nucleic Acid-Functionalized Adenoviral Vectors Targeting G-Quadruplexes in the P1 Promoter of Bcl-2 Proto-Oncogene: A New Tool for Gene Modulation in Anticancer Therapy, *Bioconjugate Chem.*, 2019, **30**, 572–582.

27 J. L. Mergny and D. Sen, DNA Quadruple Helices in Nanotechnology, *Chem. Rev.*, 2019, **119**, 6290–6325.

28 G. I. Livshits, A. Stern, D. Rotem, N. Borovok, G. Eidelshtein, A. Migliore, E. Penzo, S. J. Wind, R. Di Felice, S. S. Skourtis, J. C. Cuevas, L. Gurevich, A. B. Kotlyar and D. Porath, Long-Range Charge Transport in Single G-Quadruplex DNA Molecules, *Nat. Nanotechnol.*, 2014, **9**, 1040–1046.

29 W. Sun, D. Varsano and R. Di Felice, Effects of G-Quadruplex Topology on Electronic Transfer Integrals, *Nanomaterials*, 2016, **6**, 184.

30 A.-M. Chiorcea-Paquim, R. Eritja and A. M. Oliveira-Brett, Electrochemical and AFM Characterization of G-Quadruplex Electrochemical Biosensors and Applications, *J. Nucleic Acids*, 2018, **2018**, 5307106.

31 S. P. Liu, S. H. Weisbrod, Z. Tang, A. Marx, E. Scheer and A. Erbe, Direct Measurement of Electrical Transport through G-Quadruplex DNA with Mechanically Controllable Break Junction Electrodes, *Angew. Chem., Int. Ed.*, 2010, **49**, 3313–3316.

32 T. C. Marsh, J. Vesenka and E. Henderson, A new DNA nanostructure, the G-wire, imaged by scanning probe microscopy, *Nucleic Acids Res.*, 1995, **23**, 696–700.

33 A. B. Kotlyar, N. Borovok, T. Molotsky, H. Cohen, E. Shapir and D. Porath, Long, Monomolecular Guanine-Based Nanowires, *Adv. Mater.*, 2005, **17**, 1901–1905.

34 Y. Krishnan-Ghosh, D. Liu and S. Balasubramanian, Formation of an Interlocked Quadruplex Dimer by d(GGGT), *J. Am. Chem. Soc.*, 2004, **126**, 11009–11016.

35 K. Bose, C. J. Lech, B. Heddi and A. T. Phan, High-Resolution AFM Structure of DNA G-wires in Aqueous Solution, *Nat. Commun.*, 2018, **9**, 1959.

36 Y. Shi, H. Q. Luo and N. B. Li, A Highly Sensitive Resonance Rayleigh Scattering Method to Discriminate a Parallel-Stranded G-Quadruplex from DNA with Other Topologies and Structures, *Chem. Commun.*, 2013, **49**, 6209–6211.

37 C. Saintomé, S. Amrane, J. L. Mergny and P. Alberti, The Exception That Confirms the Rule: A Higher-Order Telomeric G-Quadruplex Structure More Stable in Sodium than in Potassium, *Nucleic Acids Res.*, 2016, **44**, 2926–2935.

38 A. Matsugami, K. Ouhashi, M. Kanagawa, H. Liu, S. Kanagawa, S. Uesugi and M. Katahira, An Intramolecular Quadruplex of (GGA)4 Triplet Repeat DNA with a G:G:G:G Tetrad and a G(:A):G(:A):G(:A):G Heptad, and Its Dimeric Interaction, *J. Mol. Biol.*, 2001, **313**, 255–269.

39 N. Ma'Ani Hessari, L. Spindler, T. Troha, W. C. Lam, I. Drevenšek-Olenik and M. Webba Da Silva, Programmed Self-Assembly of a Quadruplex DNA Nanowire, *Chem. – Eur. J.*, 2014, **20**, 3626–3630.

40 T. Ilc, P. Šket, J. Plavec, M. Webba Da Silva, I. Drevenšek-Olenik and L. Spindler, Formation of G-wires: The Role of G:C-Base Pairing and G-Quartet Stacking, *J. Phys. Chem. C*, 2013, **117**, 23208–23215.

41 P. Tóthová, P. Krafčíková and V. Víglaský, Formation of Highly Ordered Multimers in G-Quadruplexes, *Biochemistry*, 2014, **53**, 7013–7027.

42 P. Podbevšek and J. Plavec, KRAS Promoter Oligonucleotide with Decoy Activity Dimerizes into a Unique Topology Consisting of Two G-Quadruplex Units, *Nucleic Acids Res.*, 2016, **44**, 917–925.

43 T. Troha, I. Drevenšek-Olenik, M. Webba Da Silva and L. Spindler, Surface-Adsorbed Long G-Quadruplex Nanowires Formed by G:C Linkages, *Langmuir*, 2016, **32**, 7056–7063.

44 S. Kolesnikova, M. Hubálek, L. Bednárová, J. Cvačka and E. A. Curtis, Multimerization Rules for G-Quadruplexes, *Nucleic Acids Res.*, 2017, **45**, 8684–8696.

45 A. M. Varizhuk, A. D. Protopopova, V. B. Tsvetkov, N. A. Barinov, V. V. Podgorsky, M. V. Tankevich, M. A. Vlasenok, V. V. Severov, I. P. Smirnov, E. V. Dubrovin, D. V. Klinov and G. E. Pozmogova, Polymorphism of G4 Associates: From Stacks to Wires via Interlocks, *Nucleic Acids Res.*, 2018, **46**, 8978–8992.

46 N. Borbone, J. Amato, G. Oliviero, V. D'Atri, V. Gabelica, E. De Pauw, G. Piccialli and L. Mayol, D(CGGTGGT) Forms an Octameric Parallel G-Quadruplex via Stacking of Unusual G(:C):G(:C):G(:C):G(:C) Octads, *Nucleic Acids Res.*, 2011, **39**, 7848–7857.

47 V. D'Atri, N. Borbone, J. Amato, V. Gabelica, S. D'Errico, G. Piccialli, L. Mayol, G. Oliviero, V. D'Atri, N. Borbone, J. Amato, V. Gabelica, S. D'Errico, G. Piccialli, L. Mayol and G. Oliviero, DNA-Based Nanostructures: The Effect of the Base Sequence on Octamer Formation from d(XGGYGGT) Tetramolecular G-Quadruplexes, *Biochimie*, 2014, **99**, 119–128.

48 G. Oliviero, S. D'Errico, B. Pinto, F. Nici, P. Dardano, I. Rea, L. De Stefano, L. Mayol, G. Piccialli and N. Borbone, Self-

 This journal is © the Partner Organisations 2020

Open Access Article. Published on 06 July 2020. Downloaded on 12/4/2025 7:15:25 PM.
This article is licensed under a Creative Commons Attribution-NonCommercial 3.0 Unported Licence.

Assembly of G-Rich Oligonucleotides Incorporating a 3′-3′ Inversion of Polarity Site: A New Route Towards G-Wire DNA Nanostructures, *ChemistryOpen*, 2017, **6**, 599–605.

49 M. Vorlíčková, I. Kejnovská, J. Sagi, D. Renčiuk, K. Bednářová, J. Motlová and J. Kypr, Circular Dichroism and Guanine Quadruplexes, *Methods*, 2012, **57**, 64–75.

50 V. Esposito, A. Virgilio, A. Pepe, G. Oliviero, L. Mayol and A. Galeone, Effects of the Introduction of Inversion of Polarity Sites in the Quadruplex Forming Oligonucleotide TGGGT, *Bioorg. Med. Chem.*, 2009, **17**, 1997–2001.

51 R. Jin, B. L. Gaffney, C. Wang, R. A. Jones and K. J. Breslauer, Thermodynamics and Structure of a DNA Tetraplex: A Spectroscopic and Calorimetric Study of the Tetramolecular Complexes of d(TG3 T) and d(TG3T2G3 T), *Proc. Natl. Acad. Sci. U. S. A.*, 1992, **89**, 8832–8836.

52 V. Esposito, A. Virgilio, A. Randazzo, A. Galeone and L. Mayol, A New Class of DNA Quadruplexes Formed by Oligodeoxyribonucleotides Containing a 3′-3′ or 5′-5′ Inversion of Polarity Site, *Chem. Commun.*, 2005, **43**, 3953–3955.

53 C. Dalvit, Efficient Multiple-Solvent Suppression for the Study of the Interactions of Organic Solvents with Biomolecules, *J. Biomol. NMR*, 1998, **11**, 437–444.

54 M. Adrian, B. Heddi and A. T. Phan, NMR Spectroscopy of G-Quadruplexes, *Methods*, 2012, **57**, 11–24.

55 J. Vesenka and T. Marsh, The Diameter of Duplex and Quadruplex DNA Measured by Scanning Probe Microscopy, *Scanning Microsc.*, 1998, **12**, 329–342.

56 A.-M. Chiorcea-Paquim, P. V. Santos, R. Eritja and A. M. Oliveira-Brett, Self-Assembled G-Quadruplex Nanostructures: AFM and Voltammetric Characterization, *Phys. Chem. Chem. Phys.*, 2013, **15**, 9117–9124.

57 A. D. Rodrigues Pontinha, A. M. Chiorcea-Paquim, R. Eritja and A. M. Oliveira-Brett, Quadruplex Nanostructures of D(TGGGGT): Influence of Sodium and Potassium Ions, *Anal. Chem.*, 2014, **86**, 5851–5857.